Design and analysis of a high-speed micro-spindle for mechanical micromachining

Wei Li[a]*, Yinghui Ren[b], Zhixiong Zhou[c], Mingjia Liu

College of Mechanical and Vehicle Engineering, Hunan University, Changsha 410082, China

liwei@hnu.edu.cn[a]*, rebecca_ryh@163.com[b], zhouzx8@sina.com[c]

Key words: Micro-spindle, air turbine, porous bearing, micro-grinding

Abstract. Mechanical micromachining provides significant advantages over other machining techniques in part complexity, material diversity, energy consumption and cost. The existing micro-spindles does not simultaneously have ultra-high rotational speed, high rotational accuracy and compact structure. Therefore, a high-speed micro-spindle is proposed, which is driven by a radial impulse air turbine and supported by porous aerostatic bearings. The theoretical analysis models of air turbine, static radial error and dynamic response of the micro-spindle are established and the key structural parameters are attained. Two prototype micro-spindles are manufactured. Their structure are 28 mm in diameter and 45mm long and thus compact. The second improved prototype micro-spindle has a radial motion error of less than 6 μm. However, owing to the misalignment between micro tool and rotor shaft, its machining error reaches 9 μm. And the actual rotational speed during processing is less than 100,000 rpm.

Introduction

The micro-spindle is a key component of a micro-machine tool and directly determines its machining efficiency and machining quality. The most micro-spindles commercially available for micro-machine tools have a maximum rotational speed of less than 100,000 rpm. Only a few miniature spindles provide rotation speeds of exceeding 100,000 rpm. To achieve efficient material removal and desired machining quality, the micro-spindle must have ultra-high rotation speed, high rotation accuracy and compact structure. However, the micro-spindles simultaneously meeting all these requirements have rarely been developed. This study aims to develop an ultra-high speed and precision micro-spindle. The design considerations for micro-spindles are firstly discussed. Based on that, the structure configuration is designed. The theoretical analysis including calculation and simulation is carried out. The prototype micro-spindle is developed and its rotation speed, rotation accuracy, stiffness and thermal characteristics are evaluated. Finally, this prototype micro-spindle is applied to micro-grinding to verify its machining capability.

Structural configuration

The structure scheme of the micro-spindle is proposed as shown in Fig.1. It is driven by a radial impulse air turbine. To enhance the torque, two rows with a total of 12 nozzles are designed in equally spaced circumferential position. Twelve arc-shaped vanes are directly set in the middle of the rotor shaft. Both sides of the shaft are supported by porous aerostatic journal bearings. The disc arranged at the back end of the shaft is supported by two porous aerostatic thrust bearings. The tool is clamped into the shaft hole by shrink fit. The proposed micro-spindle is 28 mm in diameter and 45mm long, and thus has a compact structure.

Besides, the simple and axisymmetric structure facilitates its machining and assembly. In theory, it can achieve ultra-high speed and precision rotation, and minimize heat generation.

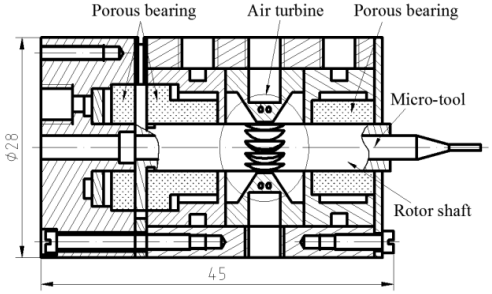

Fig. 1 Structure scheme of the proposed micro-spindle

Theoretical design of key structures

Air turbine

If the airflow in the nozzle is steady adiabatic expansion process, theoretical airflow rate u at the nozzle can be expressed as Eq. 1 according to Bernoulli equation. Consequently, the rotational speed of the wheel n can be obtained from Eq. 2 [1].

$$u=\sqrt{\frac{2\kappa}{(\kappa-1)}RT_0\left[1-\left(\frac{P_b}{P_s}\right)^{\frac{\kappa-1}{\kappa}}\right]} \tag{1}$$

$$n=60\varphi\xi u/(\pi d_m)=60\varphi\xi\sqrt{\frac{2\kappa}{(\kappa-1)}RT_s\left[1-\left(\frac{P_b}{P_s}\right)^{\frac{\kappa-1}{\kappa}}\right]}/(\pi d_m) \tag{2}$$

Where κ is specific heat (1.4 for air), R gas constant (287.05 J•(K•kg)$^{-1}$), T_s absolute temperature, P_b back pressure, P_s supply pressure, φ airflow loss coefficient around (0.92-0.98), ξ turbine speed efficiency around (0.47-0.6), d_m turbine diameter.

According to Eq. 3, the rotational speed obviously increases with the supply pressure. When the supply pressure increases to 0.44 MPa, the turbine speed can reach 500,000 rpm under a turbine speed efficiency of 0.47.

Supporting bearing

The CFD software Workbench-Fluent is used to analyze the performance of porous aerostatic bearings in this study. The established simulation model and computed pressure distribution are shown in Fig. 2. The porous medium domain is defined by viscous resistance and inertial resistance. According to the simulation result, an average film thickness of 8 μm is designed for the journal porous aerostatic bearing of the micro-spindle. The thrust porous bearing is also theoretically analyzed with software Workbench-Fluent and the zone and boundary conditions are same with that of above journal porous bearing. It is 6 mm in inner diameter, 16 mm in outer diameter and 3 mm thick. Considering both the performance requirement and machining capability, an average of 8 μm is designed for the thrust porous aerostatic bearing of the micro-spindle. When its eccentricity increases to 1 μm, the load capacity is 11.05 N.

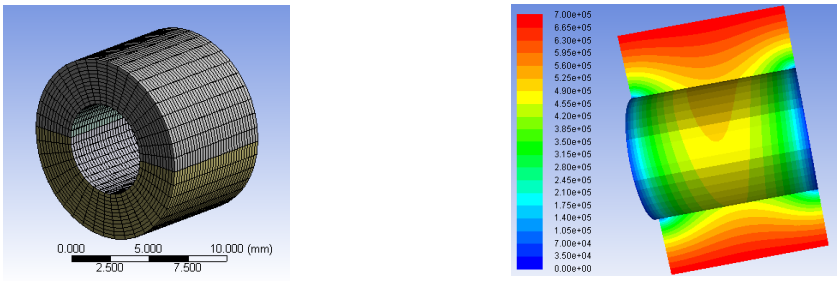

(a) Simulation model (b) Pressure distribution

Fig. 2. Simulation of journal porous aerostatic bearing

Theoretical analysis of static and dynamic characteristics

Static radial error

Based on the fundamental theory of material mechanics, the spindle shaft and the micro-tool after assembly can be simplified to simply supported beam and cantilever beam as shown in Fig. 3. The total radial deformation of the micro-tool tip is the sum of deformation δ_1 as cantilever beam, deformation δ_2 as simply supported beam, deformation δ_3 caused by front bearing and deformation δ_4 caused by back bearing. According to displacement superposition principle, the deformation of the micro-tool tip δ can be obtained by Eq. 3.

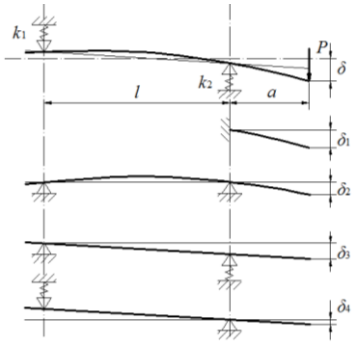

Fig. 3. Deformation schematic diagram of micro-spindle rotor shaft and micro-tool

$$\delta = \delta_1 + \delta_2 + \delta_3 + \delta_4 = P[\frac{a^3+3ta^2+3t^2a}{3E_rI_a} + \frac{t^3}{3E_tI_t} + \frac{la^2}{3E_rI_l} + \frac{1}{k_2}\left(1+\frac{a+t}{l}\right)^2 + \frac{1}{k_1}\left(\frac{a+t}{l}\right)^2 \quad (3)$$

Where P is the radial cutting load, a overhanging length of spindle shaft, l supporting span, E_r elastic modulus of spindle shaft, I_a inertia moment of overhanging section of spindle shaft, I_l inertia moment of span section of spindle shaft, t overhanging length of tool, E_t elastic modulus of tool, I_t inertia moment of tool, k_1 stiffness of back bearing, k_2 stiffness of front bearing.

The rotor shaft is made of steel 9Cr18 and the micro-tool cemented carbide. According to above calculation model, a shaft span length of 28mm is designed for the micro-spindle. With this shaft span length, the tool radial error at a tool overhanging length of 5 mm is 0.9 μm and at a tool overhanging length of 10 mm it increases to 1.4 μm.

Dynamic characteristics

The bearing-shaft-tool system was divided into rotor shaft section, connection section of rotor shaft and tool and tool section as shown in Fig. 4. Its dynamic response is attained by coupling method of multipoint response.

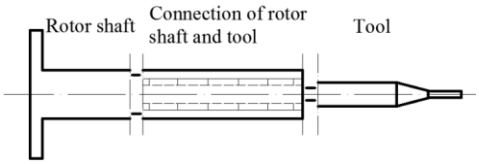

Fig. 4 Schematic diagram of rotor system

The rotor shaft and tool are simplified into several Timoshenko beams. The frequency response of whole part is obtained by rigidly coupling the response of single Timoshenko. The response equations of Timoshenko beam endpoints are given by *H*, *N*, *L* and *P* as shown in Eq. 4. The functions of *H*, *N*, *L* and *P* have been given by other literatures such as Ref. [2]. Therefore, the response matrix of single beam can be obtained by Eq. 5.

$$\begin{aligned} y_i &= H_{ij} f_j \ , \quad \theta_i = N_{ij} f_j \\ y_i &= L_{ij} m_j \ , \quad \theta_i = P_{ij} m_j \end{aligned} \tag{4}$$

$$[A] = \begin{bmatrix} A_{11} & A_{12} \\ A_{21} & A_{22} \end{bmatrix} \tag{5}$$

Where y, θ are linear displacement and angular displacement, respectively, f and m the force and torque acting on the endpoint, i and j the corresponding endpoints. $A_{11} = \begin{bmatrix} H_{A_{11}A_{11}} & L_{A_{11}A_{11}} \\ N_{A_{11}A_{11}} & P_{A_{11}A_{11}} \end{bmatrix}$, and so are A_{12}, A_{21} and A_{22}.

If the response matrix of another connected beam are *B*, the response matrix *C* of two coupling beams is

$$C = \begin{bmatrix} C_{11} & C_{12} \\ C_{21} & C_{22} \end{bmatrix} \tag{6}$$

Where $[C_{11}]=[A_{11}]-[A_{12}][[A_{22}]+[B_{11}]]^{-1}[A_{21}]$, $[C_{12}]=[A_{12}][[A_{22}]+[B_{11}]]^{-1}[B_{12}]$,
$[C_{21}]=[B_{21}][[A_{22}]+[B_{11}]]^{-1}[A_{21}]$, $[C_{22}]=[B_{22}]-[B_{21}][[A_{22}]+[B_{11}]]^{-1}[B_{12}]$.

The bearing is simplified into spring damping support located in the end of the beam as shown in Fig. 5. By combining Eq. 5 with Eq. 6, the specific expression of response matrix is given by Eq. 7.

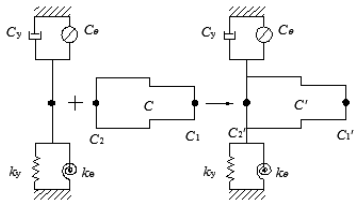

Fig. 5 Model of coupling beam with supporting bearing

$$[\alpha_C] = \begin{bmatrix} H_{C_1C_1} & H_{C_1C_2} & L_{C_1C_1} & L_{C_1C_2} \\ H_{C_2C_1} & H_{C_2C_2} & L_{C_2C_1} & L_{C_2C_2} \\ N_{C_1C_1} & N_{C_1C_2} & P_{C_1C_1} & P_{C_1C_2} \\ N_{C_2C_1} & N_{C_2C_2} & P_{C_2C_1} & P_{C_2C_2} \end{bmatrix} \tag{7}$$

The connection section of rotor shaft and tool also can be simplified to several Timoshenko beams. The end and middle points are chose as coupling points. They corresponds to three points of the tool and that of rotor shaft as shown in Fig. 6. The translation and rotation deformation of the six points can be calculated by Eq. 8.

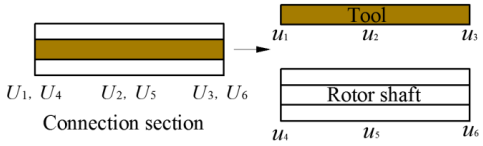

Fig. 6 Model of connection section of rotor shaft and tool

$$\left.\begin{aligned} &u_1=R_{11}q_1+R_{12}q_2+R_{13}q_3,\quad u_2=R_{21}q_1+R_{22}q_2+R_{23}q_3,\\ &u_3=R_{31}q_1+R_{32}q_2+R_{33}q_3,\quad u_4=R_{44}q_4+R_{45}q_5+R_{46}q_6,\\ &u_5=R_{54}q_4+R_{55}q_5+R_{56}q_6,\quad u_6=R_{64}q_4+R_{65}q_5+R_{66}q_6. \end{aligned}\right\} \tag{8}$$

where translation/rotation $u_1=\{y_i\ \theta_i\}^{\mathrm{T}}$, force/torque $q_i=\{f_i\ m_i\}^{\mathrm{T}}$, frequency response function $R_{ij}=\begin{bmatrix}H_{ij} & N_{ij}\\ L_{ij} & P_{ij}\end{bmatrix}$.

Based on the established response model, the first frequency response is obtained with the software Matlab and showed in Fig. 7. The first frequency is 4200 Hz and the corresponding critical rotational speed 252000 rpm. The rotor system supported by aerostatic bearing may pass through the first critical speed domain. The second frequency is 730,000 Hz and the corresponding critical rotational speed far more than the 500,000 rpm.

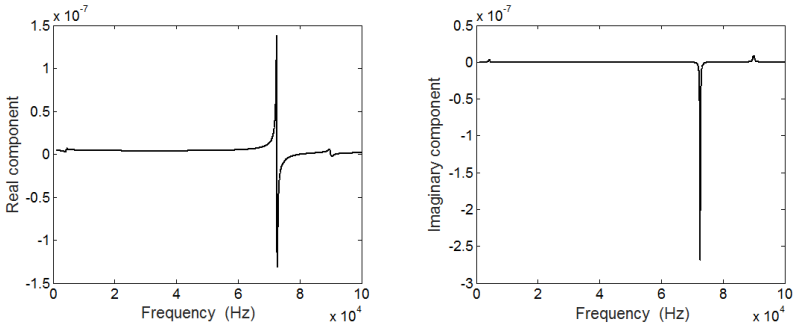

Fig. 7 The first frequency response curve of micro-spindle system

Prototype micro-spindles and their performance

The first prototype micro-spindle is developed and showed in Fig. 8(a). But the arrangement of air inlets is not convenient and affects the installation of micro-spindle on the micro-machine tool. Consequently, the micro-spindle is improved and shown in Fig. 8(b). The air inlets are arranged at the end of the micro-spindle, which make the micro-spindle compact and elegant.

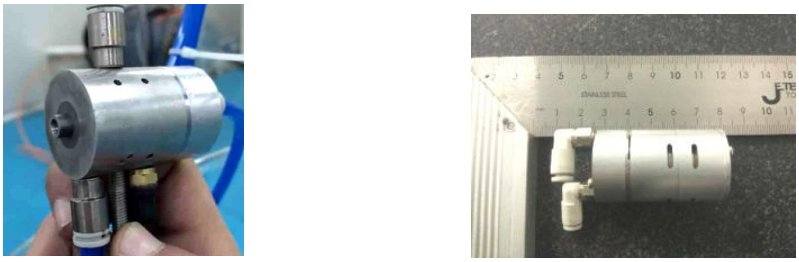

(a) The first prototype (b) Improved prototype

Fig. 8 Prototype micro-spindles

The micro-spindle does not pass through the first critical speed, which results from not

only the residual unbalance of rotor shaft, but also low load capacity of porous bearing. The radial motion error of the micro-spindle is tested and less than 6 μm as shown in Fig. 9(a). The processing performance is tested in the duralumin 6061 as shown in Fig. 9(b). The actual rotational speed during processing is less than 100,000 rpm. The used micro-grinding toolis 0.514 mm in tip diameter whereas the machined micro-slot is 0.523 mm in width. Their difference is larger than the radial motion error of micro-spindle. It is attributed to the misalignment between the micro-grinding tool and the rotor shaft.

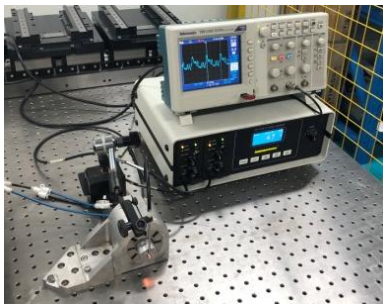

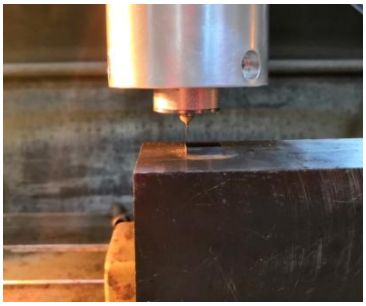

(a) Testing radial motion error (b) Micro-grinding

Fig. 9 Measurement of radial motion error and actual micro-grinding

Summary

A high-speed micro-spindle is proposed, which is driven by a radial impulse air turbine and supported by porous aerostatic bearings. It is 28 mm in diameter and 45mm long and thus has a compact structure. Two prototype micro-spindles are manufactured. The second improved prototype micro-spindle has a radial motion error of less than 6 μm. However, owing to the misalignment between micro tool and rotor shaft, its machining error reaches 9 μm. And the actual rotational speed during processing is less than 100,000 rpm. Consequently, the micro-spindle needs further improvement.

Acknowledgements

The presented work is funded by the National Science Foundation of China (51505140, 51675170), China Postdoctoral Science Foundation (2016T90749, 2015M570676), and Fundamental Research Funds for the Central Universities.

References

[1] Wei LI. Research on key technology of high speed and precision micro-spindle driven by air [D]. Changsha: Hunan University, 2014 (in Chinese).

[2] J D Aristizabal-Ochoa. Timoshenko beam-colun with generalized end conditions and nonclassi-cal modes of vibration of shear beams. Journal of engineering mechanics [J]. 2004, 130(10): 1151-1159.